Materials and Structures
DOI 10.1617/s11527-007-9226-0

ORIGINAL ARTICLE

Textile reinforced mortar (TRM) versus FRP as strengthening material of URM walls: out-of-plane cyclic loading

Catherine G. Papanicolaou · Thanasis C. Triantafillou · Myrto Papathanasiou · Kyriakos Karlos

Received: 2 June 2006 / Accepted: 19 January 2007

Abstract The application of a new structural material, namely textile reinforced mortar (TRM), as a means of increasing the load carrying capacity and deformability of unreinforced masonry walls subjected to cyclic out-of-plane loading is experimentally investigated in this study. The effectiveness of TRM overlays is evaluated in comparison to the one provided by fiber reinforced polymers (FRP) in the form of overlays or near-surface mounted (NSM) reinforcement. TRM systems may be considered as alternative to FRPs, tangling with some of the drawbacks associated with the application of the latter without compromising performance. Medium-scale tests were carried out on 12 masonry walls subjected to out-of-plane bending. The parameters under investigation comprised mortar-based versus resin-based matrix materials, the number of layers, the orientation of the moment vector with respect to the bed joints and the performance of TRM or FRP jackets in comparison to NSM strips. It is concluded that TRM jacketing provides substantial increase in strength and deformability. Compared with their epoxy-resin counterparts (FRP), TRM may result in generally higher effectiveness in terms of strength and deformability. NSM strips offer lower strength but higher deformability, due to controlled debonding. From the results obtained in this study it is believed that TRMs comprise an extremely promising solution for the structural upgrading of masonry structures under out-of-plane loading.

Keywords Textiles · Mortars · TRM · FRP · Out-of-plane cyclic loading · Seismic retrofitting

C. G. Papanicolaou (✉) · T. C. Triantafillou · M. Papathanasiou · K. Karlos
Department of Civil Engineering, University of Patras, Patras 26500, Greece
e-mail: kpapanic@upatras.gr

1 Introduction and background

Unreinforced masonry bearing wall construction, commonly termed URM, is one of the oldest construction types found worldwide. URM walls have been proven to be prone to failure during high or even moderate intensity earthquakes or high wind pressure, and, therefore, they represent a significant hazard to life safety. A causal breakdown of earthquake fatalities for the last century's second half revealed that almost 60% of the induced life losses were attributed to URM failures [1]. Moreover, structural decay due to ageing or cumulative seismic-induced damage poses a direct threat to the preservation and safeguarding of historical structures that comprise an important part of many countries' cultural heritage. Thereby, there is a tremendous and

urgent need for upgrading existing URM structures, both in seismic areas, where structures designed according to old seismic codes have to meet upgraded performance levels demanded by current seismic design standards, and in non-seismic areas, e.g. due to change of usage and/or the introduction of more stringent design requirements.

Numerous techniques have been developed aiming at increasing the strength and/or ductility of URM walls, including the use of metallic or polymeric grid—reinforced surface coatings, shotcrete overlays, internal or external prestressing with steel ties, externally bonded fiber reinforced polymers (FRP, such as epoxy-bonded strips or in-situ impregnated fabrics) and near-surface mounted (NSM) FRP reinforcement. FRP-based strengthening and/or seismic retrofitting techniques have been well-established in the civil engineering community due to favorable properties offered by these materials, such as high strength and stiffness to weight ratio, corrosion resistance, ease and speed of application and minimal change in the geometry.

Studies on the use of FRP as strengthening materials of masonry have been numerous. These studies have dealt with strengthening of: (a) walls, through external prestressing (e.g. [2]); (b) columns, through confinement (e.g. [3, 4]); (c) walls subjected to in-plane loading, through externally bonded strips or overlays (e.g. [5–14]); (d) walls subjected to out-of-plane loading, through externally bonded strips or overlays (e.g. [8, 15–21]); (e) walls, through near-surface mounted reinforcement (e.g. [22, 23]); and (f) vaults and arches (e.g. [24, 25]).

Despite the many advantages associated with the use of FRPs, the relevant strengthening techniques are not entirely problem-free. Some drawbacks are attributed to the organic resins used to bind or impregnate the fibers and may be summarized as follows: (a) poor behavior of epoxy resins at temperatures above the glass transition temperature (as a result, special and expensive fire protection measures are often called for); (b) relatively high cost of epoxies; (c) potential hazards for the manual worker (especially when proper ventilation of work space is not ensured: hardener vapors may cause respiratory problems, or irritation and inflammation of sensitive skin areas); (d) application of FRPs on wet surfaces or low temperatures is practically not possible; (e) lack of vapor permeability; (f) incompatibility of epoxy resins and some substrate materials (e.g. clay); and (g) difficulty to conduct post-earthquake assessment of the damage suffered by the masonry behind the FRP. In addition, certain properties of clay masonry, such as the porosity and surface unevenness and/or roughness, which affect the epoxy-brick bond behavior, as well as restrictions related to intervention strategies for historic masonry buildings (e.g. requirements for reversibility), may possibly inhibit the success of FRP application.

One possible solution to the above problems would be the replacement of organic binders with inorganic ones, e.g. cement-based mortars, leading to the replacement of FRP with fiber reinforced mortars (FRM), sometimes also referred to as cementitious composite systems. These materials have a relatively long-term record in structural engineering, especially in the development of thin section products [26], but when they contain continuous fibers they fail to ensure their efficient use. This weakness is the consequence of the mortar's granularity, which hinders penetration and impregnation of fiber sheets. Therefore, cement-based matrices lack the fundamental property of binders (such as epoxies), which is the ability to penetrate and wet individual fibers. The first study identified by the authors in the field of masonry strengthening with FRM was that of [27]. In this study a masonry wall constructed from sand–lime bricks and strengthened with a carbon fiber cement matrix system (three layers of unidirectional carbon fabric in a polymer-modified cement binder) was tested under out-of-plane loading and exhibited a considerable increase in strength compared with the unstrengthened wall.

Bond conditions in cementitious composites could be improved and fiber–matrix interactions could be made tighter when continuous fiber sheets are replaced by textiles. These materials comprise fabric meshes made of long woven, knitted or even unwoven fiber rovings in at least two (typically orthogonal) directions. The density,

that is the quantity and the spacing, of rovings in each direction can be controlled independently, thus affecting the mechanical characteristics of the textile and the degree of penetration of the mortar matrix through the mesh openings (which in turn determines the degree of the mechanical interlock achieved).

Although research on the use of textile meshes as reinforcement of cementitious products commenced in the early 1980s, developments in this field progressed rather slowly until the late 1990s. But during the past five years or so, the research community has put a considerable effort on the use of textiles as reinforcement of cement-based products, primarily in new constructions (e.g. [28–32]). In the field of strengthening, textiles combined with mortars have been used as external reinforcement of concrete by [33–35] for flexural and shear strengthening; by [36, 37] for shear strengthening; and by [36, 38] for confinement.

Recently, textiles combined with mortars were used by [39] as a means of increasing the strength of tuff masonry wallettes tested in diagonal compression and by [40, 41] in the form of confining jackets for small scale rectangular column-type specimens tested in uniaxial compression. In this study the authors go one step further: they test under cyclic loading conditions, for the first time, masonry walls strengthened on both sides with textile reinforced mortars (TRM), and they compare the efficiency of TRM jackets with their FRP counterparts. Additional comparisons are also made with respect to NSM reinforcement. The results concerning out-of-plane bending are reported in this paper, whereas those on in-plane loading are presented in [42].

2 Experimental program

2.1 Scope and method

The main objective of the experimental program was to provide an understanding on the effectiveness of externally bonded TRM as strengthening materials of unreinforced masonry walls subjected to out-of-plane cyclic bending. The investigation was carried out on two series of medium-scale, single-wythe, fired clay brick wallettes comprising running bond courses: (a) Series A specimens measured (approximately) 1300 mm in height and 400 mm in width (Fig. 1a) and were tested out-of-plane, such that the plane of failure would form parallel to the bed joints (e.g. piers subjected to out-of-plane bending); (b) Series B specimens measured (approximately) 400 mm in height and 1300 mm in width (Fig. 1b) and were tested out-of-plane, such that the plane of failure would form perpendicular to the bed joints (e.g. as in vertically supported walls loaded out-of-plane). All specimens were constructed in the laboratory by an experienced mason using perforated bricks ($185 \times 85 \times 60$ mm—Fig. 1c), with the perforations running in parallel to the units' length. For all specimens, the first row of bricks was laid on a 10 mm thick horizontal layer of mortar and all joints (bed and head) were approximately 10 mm thick.

Two major parameters were considered in the investigation, namely the use of inorganic mortar versus resin-based matrix material for the textile reinforcement and the number of textile layers (one or two layers, applied on both sides). In addition, a small part of this experimental study focused on the use of near-surface mounted CFRP strips, which were placed along bed joints.

It is noted that the strengthening schemes applied on wall specimens for the purposes of this investigation did not necessarily intend to account for realistic fiber quantities that could be used in real interventions, but rather to compare such

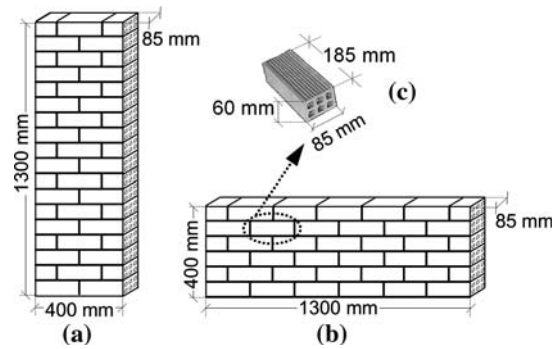

Fig. 1 (**a**) Series A specimens; (**b**) Series B specimens; and (**c**) 6-hole clay bricks

quantities in combination with inorganic versus polymeric matrices.

2.2 Test specimens and materials

All specimens were constructed using ridge-faced, 6-hole, horizontally perforated clay bricks, supplied by a local manufacturer, and a general purpose masonry cement mortar. Series A included five different designs: the control specimen (without strengthening), two specimens each symmetrically strengthened with one or two layers of textile bonded with a commercial polymer-modified cement mortar and two identical specimens where the textiles were bonded with a two-part epoxy adhesive. Series B included the same five designs as Series A, but was also complemented by two more: a specimen with two NSM CFRP strips per side, placed along slots formed in the second and fourth bed joints, and another specimen with three NSM CFRP strips per side, placed along every other bed joint (first, third, fifth). As a result, a total of 12 tests were performed. Specimens are given the notation Y_XN, where Y denotes the specimens' Series (A or B), X denotes the type of binder used (M for mortar and R for resin) and N denotes the number of layers (1 or 2). The designations C, NSM2 and NSM3 (in place of XN) are used to distinguish the control specimens and the ones receiving two and three NSM strips (per side), respectively. All types of specimens used in this study are summarized in the first column of Table 1.

The mean compressive strength of the masonry units in directions parallel and perpendicular to the perforations was derived from three compressive tests in each case. The bearing surfaces of the individual brick specimens were capped using a self-leveling, rapid-hardening cement mortar. The average values obtained were 8.9 MPa and 3.7 MPa for directions parallel and perpendicular to the perforations, respectively.

The cement:lime:sand proportions in the mortar used to bind the bricks were roughly 1:2:10, by volume, and the water to cement ratio was in the order of 0.8, by weight. The mortar strength was obtained through flexural and compression testing according to [43], using a servohydraulic MTS testing machine. Flexural testing was carried out on $40 \times 40 \times 160$ mm hardened mortar prisms, at an age of 28 days. The prisms were: (i) prepared in steel moulds with three identical compartments, so that three specimens were available for each day of the walls' construction period (spanning three days); (ii) cured in the laboratory until testing, in conditions identical to those for the wall specimens; and (iii) subjected to three-point

Table 1 Summary of test results

Specimen notation	Peak load (kN)		Mid-span displacement at failure (mm)[a]		Cumulative dissipated energy (kNmm) at cycle		Failure mode (Failure direction)
	Push	Pull	Push	Pull	4	10	
Series A							
A_C	~0.66	–	–	–	–	–	Failed during transport
A_R1	10.02	9.28	4.45	11.14	32.32	223.68	Flexure-shear (Push)
A_R2	12.94	11.72	3.75	4.35	32.09	248.77	Flexure-shear (Push)
A_M1	12.22	10.02	10.73	11.03	32.69	194.10	Flexure-shear (Push)
A_M2	15.15	12.45	6.05	6.25	38.60	290.51	Flexure-shear (Push)
Series B							
B_C	3.36	–	0.99	–	–	–	Flexure
B_R1	21.45	17.82	9.90	11.02	61.84	383.97	Sudden FRP fracture (Pull)
B_R2	26.15	18.81	7.11	7.11	67.29	429.24	Flexure-shear (Push)
B_M1	18.31	14.42	12.92	9.45	64.18	368.75	Gradual TRM fracture (Pull)
B_M2	29.52	21.97	9.92	12.59	77.19	437.63	Flexure-shear (Push)
B_NSM2	12.95	8.54	12.62	12.14	54.93	254.64	Flexure & debonding
B_NSM3	15.87	11.96	17.16	19.89	41.70	210.88	Flexure-shear & debonding

[a] Corresponding to sudden load reduction, or to displacement at 80% of the peak load in case of gradual post-peak load reduction

bending, at a span of 100 mm, with a constant loading rate equal to 5 N/s. The peak load was recorded and used for the calculation of flexural strength. Compression testing was carried out on each of the fractured parts of the prisms used in flexural testing, by means of two 40×40 mm bearing steel platens placed on top and bottom of each specimen part, which was carefully aligned so that the load was applied to the whole width of the faces in contact with the platens. The flexural and compressive strengths obtained from this procedure were 1.17 MPa and 3.91 MPa, respectively (mean values of all prisms tested).

For the specimens receiving externally bonded strengthening, a commercial textile with equal quantity of high-strength carbon fiber rovings in two orthogonal directions was used (Fig. 2a). The fiber rovings in each direction were simply placed one on top of the other and connected through a secondary polypropylene grid (see Fig. 2b for the carbon roving architecture). Each fiber roving was 4 mm wide and the clear spacing between rovings was 6 mm. The weight of carbon fibers in the textile was 168 g/m^2 and the nominal thickness of each layer (based on the equivalent smeared distribution of fibers) was 0.047 mm. The guaranteed tensile strength of the carbon fibers (as well as of the textile, when the nominal thickness is used) in each direction was taken from data sheets of the producer equal to 3350 MPa. The elastic modulus of carbon fibers was 225 GPa.

For the specimens receiving mortar as binding material, a commercial inorganic dry binder was used, consisting of cement and polymers at a ratio 10:1, by weight. The binder to water ratio was 3.3:1, by weight, resulting in plastic consistency and good workability with a retention period of approximately half an hour in ambient temperature (20°C). The binder's flexural and compressive strengths (5.77 MPa and 31.36 MPa, respectively) were obtained from a procedure identical to the one described for the general purpose masonry mortar, using triplets of mortar prisms taken each day during the strengthening execution.

For the specimens receiving adhesive bonding a commercial structural adhesive (two-part epoxy resin with a mixing ratio 4:1 by weight) was used with a tensile strength of 30 MPa and an elastic modulus of 3.8 GPa (cured for 7 days at 23°C). The adhesive was pasty with a viscosity such that complete wetting of the fibers in the textile was possible by using a plastic roller.

For the specimens with NSM reinforcement, provision was taken during the construction phase to form grooves along the bed joints designated to receive the CFRP strips. The grooves were shaped by scraping-off part of the bed mortar, while still in fresh state. Prior to the application of the NSM strips, the grooves were thoroughly cleaned using compressed air and dampened through water spraying. Then, the slots were filled with a cement-based mortar taking care to avoid air entrapment, and the strips, which extended the full length of the (Series B) specimens, were inserted in the grooves (seated on face) until full embedment was achieved. Finally, any excess mortar was removed and the grooves' face was made even with the face of the wall using a trowel.

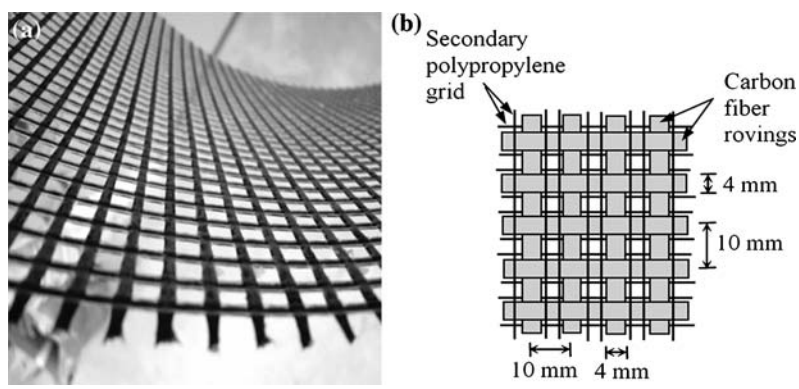

Fig. 2 (**a**) Photograph; and (**b**) architecture of bi-directional textile used in this study

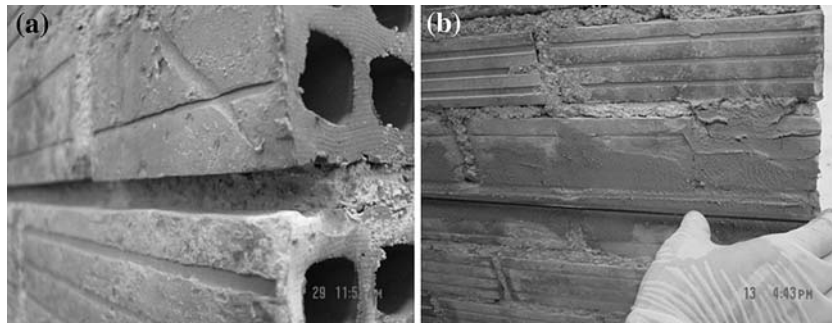

Fig. 3 (**a**) The bed slots' size allows for the complete encapsulation of the NSM strips; and (**b**) the NSM strip is being pressed in the mortar-filled slot

The basic steps of the aforementioned procedure are illustrated in Fig. 3. The mortar used to fix the NSM strips in place comprised a three-part material consisting of: liquid compounds A and B (epoxy resin suspensions) and solid compound C (cement plus cementitious materials) with a mixing ratio A:B:C equal to 1.14:2.86:17, by weight. Its consistency allowed for vertical applications, whereas its compressive and flexural strengths (as provided by the producer data sheets) were 40 MPa and 9 MPa, respectively.

Commercially available tape-like CFRP strips specifically designed for NSM strengthening were used. The strips with a cross section of 2×16 mm were furnished in 76 m long spools and consisted of carbon fibers in a bisphenol epoxy vinyl ester resin matrix. The elastic modulus and volumetric ratio of carbon fibers in the CFRP strips were equal to 225 GPa and 40%, respectively. The guaranteed tensile strength, the elastic modulus and the ultimate strain of the CFRP strips were taken from data sheets of the producer equal to 2070 MPa, 125 GPa and 0.17%, respectively. For the sake of scaling down, each NSM strip was cut in two pieces (along the length) using a thin saw; the resulting strips had a width of 7.5 mm.

Calculations of the axial stiffness for both the NSM reinforcement on each side of the walls and the textile jackets based on the contribution of fibers only ($E_{fib}A_{fib}$), gave the following results: 2700 kN or 4050 kN for two or three NSM strips and 4230 kN or 8460 kN for one or two layers of textile. These numbers indicate that the reinforcing ratio in the wallette with three NSM strips (B_NSM3) was approximately equal to that in the wallettes with one layer of the textile reinforcement (B_R1, B_M1).

In order to avoid premature failure due to handling and positioning of the unjacketed specimens (control and strengthened with NSM), a 15 mm thick layer of plaster was applied on their faces. A commercial dry cement-based mix was used following a double-coat procedure: the undercoat was forcefully thrown on the damp masonry surface (using a hand-held trowel), in order to improve adhesion, and the second coat was applied while the first one was still fresh but relatively firm. The plaster's 28-days compressive strength was approximately equal to 4 MPa.

All textile layers were applied ''as usual'', that is each specimen was first ground at points where mortar was protruding from the brickwork face and brushed clean, then dust and any loose particles were removed with high air pressure and, finally, a standard wet lay-up procedure was followed to bond the textile sheets on both sides of the walls, covering the entire surface of each side. The procedure involved the application of a bonding agent (either epoxy or mortar) on the wall surface (which was dampened for specimens receiving mortar) and the subsequent bonding of the textile by hand and roller pressure. The bonding agent was also applied in between layers and on top of the last textile layer. Application of the mortars was made in approximately 2 mm thick layers with a smooth metal trowel. The textile was pressed slightly into the mortar, which protruded through all the perforations between fiber rovings. Of crucial importance in this method, as in the case of epoxy resins, was the application of each mortar layer while the previous one was still in a fresh state. Curing of the bonding agents was achieved in room conditions. A typical photograph of the application method

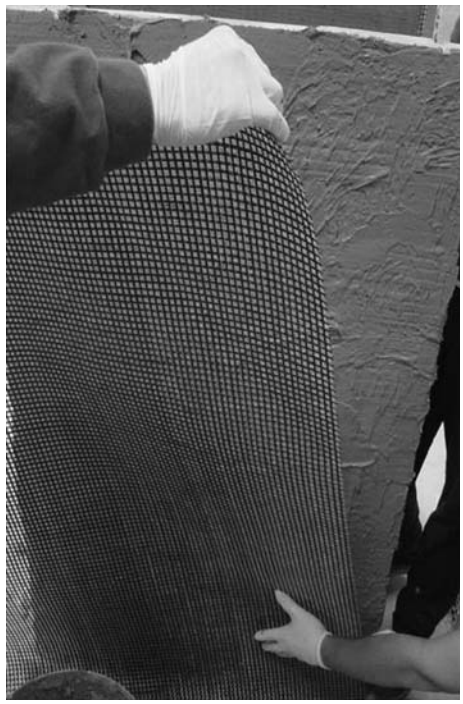

Fig. 4 Application of the textile reinforcement onto the cementitious mortar

of textile sheets combined with mortar binder on wall specimens is shown in Fig. 4.

The mean compressive strength of the walls in directions parallel and perpendicular to the bed joints was measured from three compressive tests in each case, conducted on small wall assemblages (two bricks long by six bricks high), measuring $390 \times 85 \times 420$ mm (length $\times$ width $\times$ height). These masonry prisms were constructed using the same bricks, mortar and bond type (that is running bond) as for the rest of the specimens used in the experimental program. It should be noted that all types of wall specimens were constructed and tested during the same time spans. The surfaces of these specimens in contact with the compression platens were capped using a normal strength cement mortar, in order to achieve a better load transfer. The compression tests were carried out in displacement control mode at a constant loading rate equal to 0.1 mm/s, using a 4000 kN loading capacity testing machine. Loads were measured from a load cell and displacements were obtained using external linear variable differential transducers (LVDTs) with a stroke of 5 mm. The LVDTs were mounted at mid-height, at a gauge length of approximately 130 mm. The mean values of the compressive strength, secant modulus of elasticity (at maximum stress) and ultimate strain derived from compressive loading parallel to the bed joints were 4.3 MPa, 1.94 GPa and 0.22%, respectively. The corresponding values for compressive loading perpendicular to the bed joints were 2.0 MPa, 1.70 GPa and 0.12%, respectively.

As expected, due to the different strength characteristics of the masonry walls in two orthogonal directions (perpendicular and parallel to the bed joints), the uniaxial strength of the walls in these directions was found to be different. More specifically, failure due to loading parallel to the bed joints was very brittle and resulted due to crushing of the outer brick cells. For loading perpendicular to the bed joints failure was less sudden than for the previous case and was manifested through vertical cracks running along the height of the walls, crossing the bed joints.

2.3 Test set-up, instrumentation and procedure

All strengthened specimens were subjected to cyclic out-of-plane loading using a stiff steel frame. The walls were laid horizontal (with the bonded surfaces facing upwards and downwards) and were loaded in three-point bending (Fig. 5) at a span of 1.20 m and 1.15 m for specimens of Series A and B, respectively. Two pairs of steel

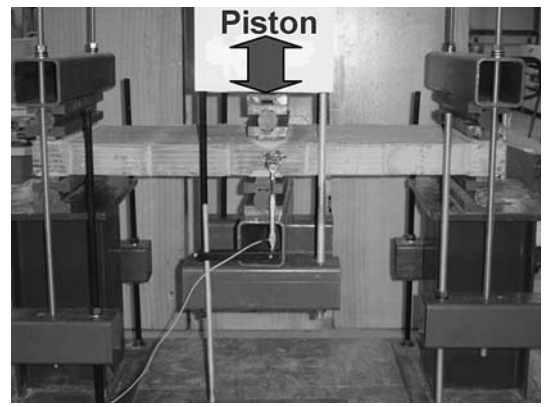

Fig. 5 Experimental setup

hinges were placed at each support (along the specimens' width, at top and bottom) and a third one was placed at mid-span (that is along the load application line). The load was applied using a vertically positioned 500 kN MTS actuator. At least one week prior to testing six 50 mm wide and 7 mm thick bands of high strength mortar had been cast on the specimens' faces along all bearing lines (three per side), in order to compensate for any surface unevenness and to ensure uniformity of load transfer.

Displacements were measured at mid-span using an external rectilinear displacement transducer (of 25 mm stroke capacity) mounted on one side of the specimen. Data from the load cell and the displacement transducers (the actuator's and the external one) were recorded using a fully computerized data acquisition system. The resulting load—mid-span displacement and load—piston displacement loops were generated by the system in real time.

All strengthened specimens were tested by applying the load in a quasistatic cyclic pattern of controlled displacements at a rate of 0.1 mm/s. The loading sequence consisted of cycles at a series of progressively increasing displacement amplitudes in both directions (push and pull). The displacement amplitude increment was 1 mm and a single loading cycle was applied for each amplitude level, as illustrated in Fig. 6. The test was run in a fully computerized manner and was completed (manually terminated by returning the piston to zero position) when the ultimate capacity of the wall was reached and a considerable load reduction was evidenced in either direction (push or pull). Control specimens were tested under monotonically applied loading, in a displacement control mode and at the same rate as for strengthened specimens.

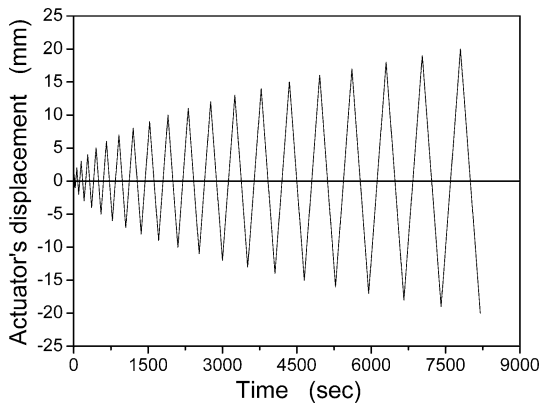

Fig. 6 Displacement history

3 Results and discussion

The results are discussed based on the load versus out-of-plane displacement response. Peak load values in the push and pull directions, P^{+}_{max} and P^{-}_{max}, mid-span displacements at failure, δ^{+}_{u} and δ^{-}_{u}, (defined as the point of the load versus mid-span displacement envelope curve where either sudden load reduction was detected, or a 20% reduction in load was noted in specimens with gradual post-peak load reduction), cumulative energy dissipation capacity, observed failure modes and loading directions when failure occurred are given in Table 1, for all specimens.

3.1 Series A—Out-of-plane-bending with plane of failure parallel to bed joints

Despite plaster rendering and careful handling, the control specimen of Series A failed under self-weight (approximately equal to 0.66 kN) during transportation to the steel frame. This was not surprising, as the tensile strength of the walls perpendicular to the bed joints was very low. All remaining specimens of Series A showed a fairly consistent behavior failing in a flexure-shear mode in the push direction. The load versus mid-span displacement hysteresis loops for Series A specimens (except for the control one) are given in Fig. 7a–d (values in the push direction, that is downward movement of the piston, are taken positive).

During the first five loading cycles, specimen A_R1 (one layer of resin-impregnated textile on each side) showed some hairline flexural cracks near the mid-span (on brick shells and along mortar joints), as well as signs of brick-bed joint debonding, the full development of which was prevented by the textile reinforcement. In the push direction of cycle 6 (piston displacement amplitude equal to 6 mm) a diagonal crack was formed and propagated towards the loading line;

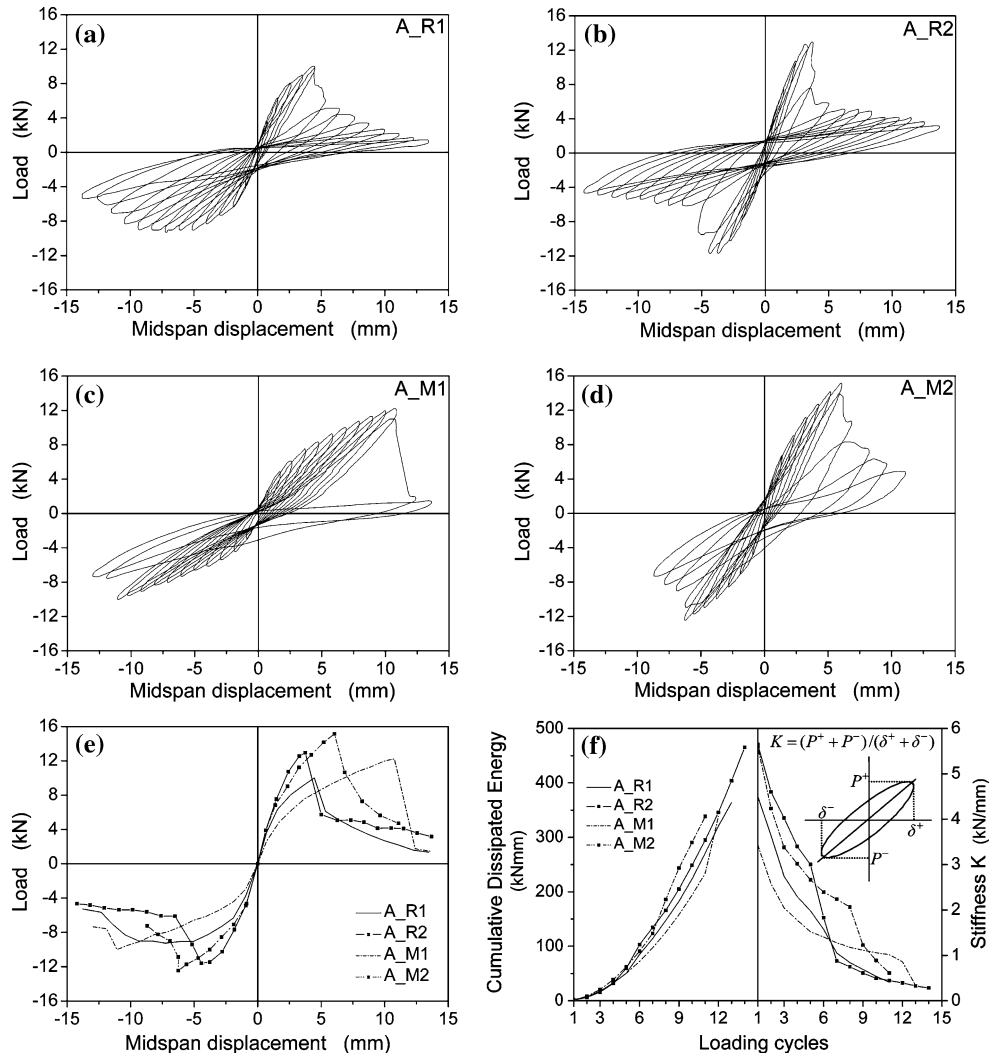

Fig. 7 Series A results: (**a**–**d**) Load versus mid-span displacement hysteresis loops; (**e**) envelope curves; (**f**) cumulative energy and stiffness versus loading cycles

upon load reversal, a mirror—but less extensive—crack was formed (Fig. 8a). This resulted in notable strength and stiffness degradation in the push direction, whereas in the pull direction the respective degradations were less pronounced. Whilst the x-shaped cracking pattern, typical of

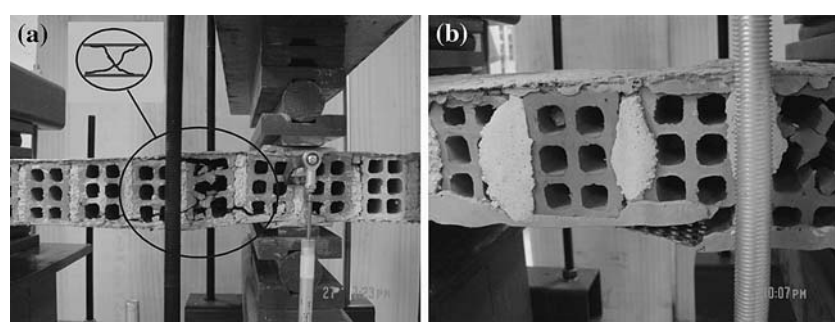

Fig. 8 (**a**) Diagonal cracking of masonry walls; (**b**) debonding of the jacket at large displacements

fully reversed loading conditions, was nearly symmetrical to the specimen's longitudinal axis of symmetry, this was not the case with respect to the specimen's centerline, because damage was localized in one of the shear spans. At higher displacement amplitudes the cracks caused the brick webs to gradually crush and the textile layer to debond from the core brickwork. Excellent brick to textile bond was observed as the outer brick shells were firmly attached to the debonded reinforcement layer. The maximum recorded load for specimen A_R1 was 10.02 kN in the push direction and the corresponding mid-span displacement was 4.45 mm.

A similar to the A_R1 behavior was observed for the specimen receiving two layers of resin-impregnated textiles on each side (A_R2). Up to the fifth displacement cycle no visible damage was detected, although stretching of the layers and probable minor local failures were manifested by the sounds of breaking resin. The cracking progress in the following displacement cycles was almost identical to that of specimen A_R1. Due to the formation of large diagonal cracks, the load capacity of the specimen was drastically reduced. Subsequent displacement cycles caused the complete crushing of the brick webs adjacent to the cracks and resulted in the nearly independent action of the reinforcing layer. As a result of a rather symmetrical damage pattern induced both in the push and pull directions, strength and stiffness degradation characteristics for specimen A_R2 were similar in both loading directions. Compared to the specimen receiving a single layer of epoxy-bonded textile per side, specimen A_R2 reached a higher failure load (12.94 kN in the push direction), corresponding to a gain of 30%. Additionally, as can be seen in Fig. 7e by comparison of the envelope curves of specimens A_R1 and A_R2, the latter is characterized by a steeper ascending branch and reduced deformability: the mid-span displacement at failure for specimen A_R2 was found to decrease by 16% in comparison to specimen A_R1 (in the push direction).

For the specimen receiving one layer of mortar-impregnated textile on each side (A_M1), as displacement amplitudes increased, debonding of brick-bed joint interfaces close to the mid-span was detected (within a distance spanning three to four courses on each side of the load application line). Nevertheless, until the onset of the tenth displacement cycle the panel showed no other signs of severe damage. Contrary to the resin, the cementitious matrix allowed the formation of almost evenly distributed fine cracks on the coated surface, parallel to the bed joints. Hence, the low tensile capacity of the cementitious matrix and the resulting distributed cracking led to a more compliant response, enabling the wall to develop higher deflections at failure and to fail at a higher load. Failure of the wall occurred during the eleventh cycle, through the formation of diagonal cracks, as in the case of specimen A_R1. At larger displacement reversals the bricks adjacent to the crack crushed and the crack propagated through the masonry—TRM interface, causing controlled debonding of the textile reinforcement (Fig. 8b). This specimen failed at a load of 12.22 kN (in the push direction) with a corresponding displacement of 10.73 mm. Therefore, in comparison with its resin-impregnated counterpart, the TRM-strengthened wall displayed a 22% increase in strength and a 140% increase in deformability.

The behavior of specimen A_M2 resembled the one of specimen A_R2. Although less stiff than its resin-impregnated counterpart, specimen A_M2 failed (also due to diagonal cracking) at a higher load (15.15 kN in the push direction—the highest for Series A specimens), accounting for an increase of 17% in comparison to A_R2; when compared to specimen A_M1, the peak load increase amounted to 25%. In terms of displacement capacity, specimen A_M2 failed at 61% higher and 44% lower mid-span displacement compared with walls A_R2 and A_M1, respectively.

Overall, it is concluded that textile-reinforced mortar jacketing was extremely effective, outperforming FRP jacketing. On the basis of strength and deformability, one may quantify the effectiveness of TRM jacketing with respect to its FRP counterpart by dividing the relative capacities, as mentioned above. These ratios appear to be consistently high, in the order of 1.2 for strength (actually 1.22 for one layer of textile and 1.17 for two layers) and on average 2.0 for deformability

(2.41 for one layer of textile and 1.61 for two layers).

By comparison of the cumulative dissipated energies given in Fig. 7f and Table 1 (computed by summing up the area enclosed within the load versus piston displacement curves), it is concluded that, in general, the energy dissipation capacity of the two strengthening schemes (FRP versus TRM) is comparable. Finally, the comparison of the stiffness versus loading cycles shown also in Fig. 7f confirms the slightly more compliant behavior of TRM-jacketed masonry versus its FRP counterpart at early stages of deformation; but this behavior reverses at larger deformations, when FRP-strengthened specimens have already failed while their TRM counterparts are still intact.

3.2 Series B—Out-of-plane-bending with plane of failure perpendicular to bed joints

The control specimen of Series B failed under monotonic loading at a maximum load of 3.36 kN following the formation of a single crack at the brick-head joint interfaces closest to the loading line (mid-span). Visual inspection revealed that the crack propagated stepwise through some of the bed joints (in the longitudinal direction), without causing fracture of the bricks.

Specimens B_R1, B_R2, B_M1 and B_M2 experienced diagonal cracking during the early cycles of the response, as was the case with the specimens in Series A. This cracking pattern became critical and marked the failure mechanism of B_R2 and B_M2 (that is with two layers of textile on each side); but specimens B_R1 and B_M1 (with one layer of textile) failed due to tensile fracture of the textile at mid-span. The load versus mid-span displacement hysteresis loops for Series B specimens with textile-based jackets are given in Fig. 9a–d; and more details about each specimen are given next.

Following the formation of diagonal cracking close to the maximum moment line, the FRP jacket of specimen B_R1 failed suddenly in tension during the 13th displacement cycle in the pull direction (Fig. 10a). Tensile fracture of the FRP led to the complete loss of the wall's load bearing capacity and the test was thus terminated. The recorded peak loads in the push and pull direction were 21.45 kN and 17.82 kN, respectively, and the corresponding displacements at failure were 9.90 mm and 11.02 mm. Compared with B_R1, specimen B_R2 reached a 22% higher peak load (in the push direction), failing due to diagonal cracking adjacent to the load application line, and a 28% lower displacement at failure; this difference in deformability is attributed to the higher post-cracking stiffness of B_R2 compared with B_R1, due to the increased thickness of the strengthening jackets. The respective numbers in the pull direction were 6% and 35%.

Specimen B_M1 failed due to gradual tensile fracture of the TRM jacket in the pull direction, at a load of 14.42 kN and a displacement of 9.45 mm. In comparison with its resin-based counterpart (B_R1), this specimen displayed a 19% reduction in strength (in the pull direction) and a 14% reduction in displacement at failure. This result indicates that if failure of the strengthened wall is controlled by tensile fracture of the jacket, TRM is less effective than its FRP counterpart in terms of both strength and deformability, a conclusion which is in agreement with findings obtained recently for TRM jackets used for confinement [38] as well as shear strengthening [37].

Specimen B_M2 (with two layers of textile in the TRM jacket) behaved similarly to B_R2, that is failure occurred due to diagonal cracking. The failure load was 29.52 kN and the displacement at failure was 9.92 mm (in the push direction). In comparison with B_R2 these values are 13% and 39% higher. Finally, when compared with B_M1, the results for specimen B_M2 indicate a 52% increase in strength and a 33% increase in displacement at failure (in the pull direction).

The two walls strengthened with NSM FRP strips displayed different behavior characteristics. Specimen B_NSM2 developed extensive flexural cracking mainly at mid-span, followed by controlled debonding of the NSM strips; this became evident through the development of longitudinal splitting cracks in the positions of NSM strips along the bed joints (Fig. 10b). The peak load and ultimate displacement (Fig. 9e) for this wall were 12.95 kN and 12.62 mm, respectively (in the push direction).

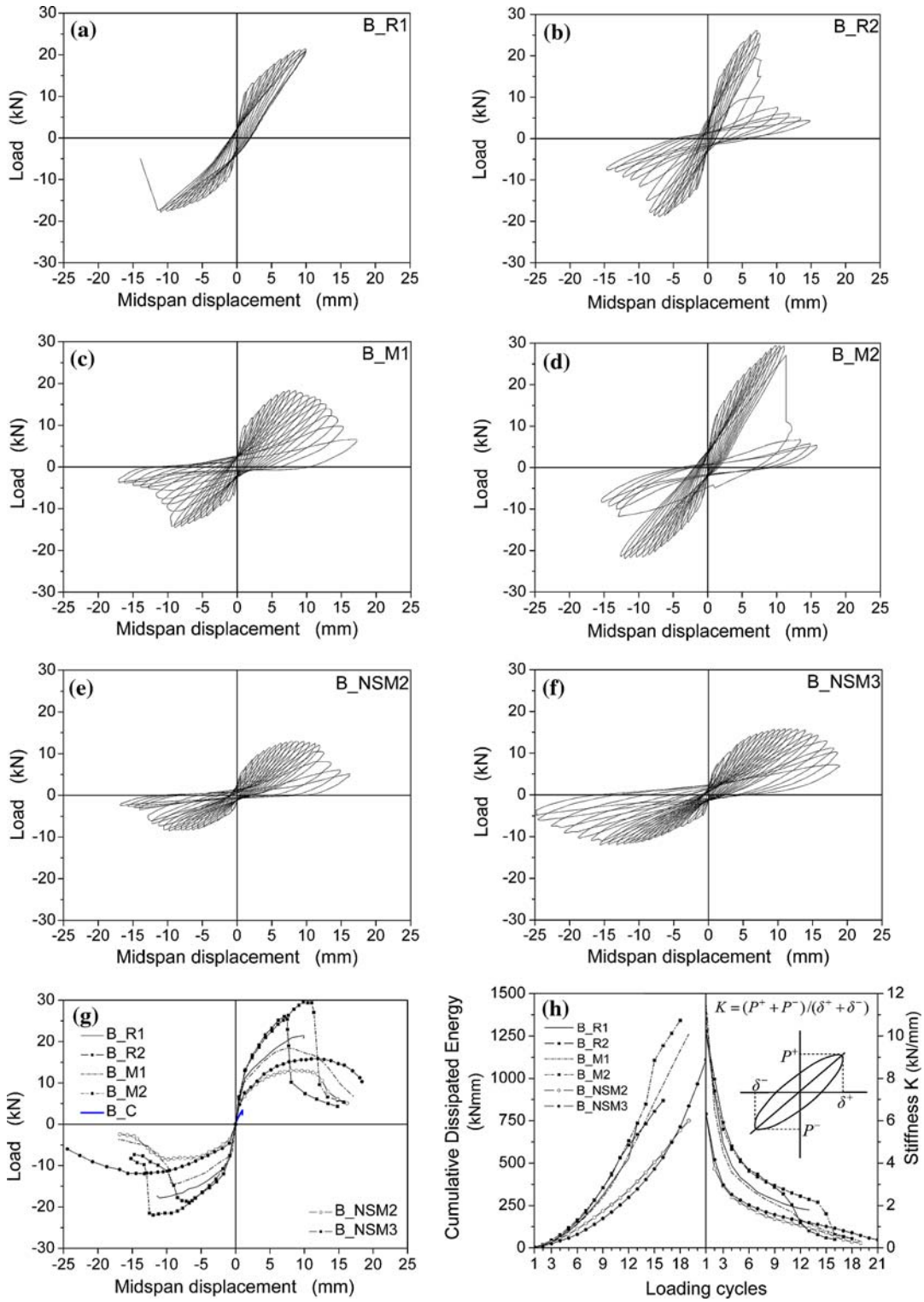

Fig. 9 Series B results: (**a**–**f**) Load versus mid-span displacement hysteresis loops; (**g**) envelope curves; (**h**) cumulative energy and stiffness versus loading cycles

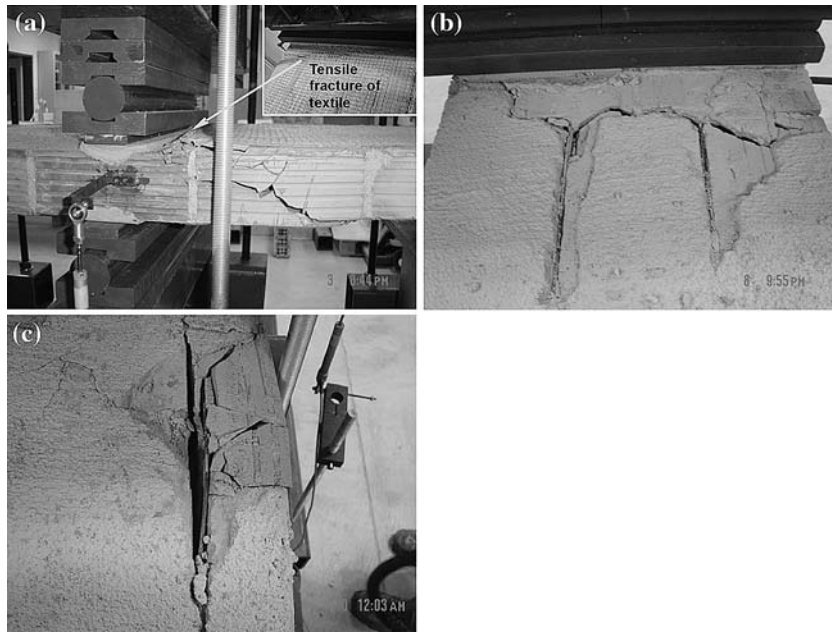

Fig. 10 (**a**) Tensile fracture of the textile (specimens B_R1 and B_M1); (**b**) flexural cracking of the wall and debonding of NSM strips (specimen B_NSM2); (**c**) severe damage of masonry and buckling of NSM strip

Specimen B_NSM3 developed similar behavior characteristics, except that flexural-shear cracking was a bit more distributed. The peak load and ultimate displacement for this specimen were 15.87 kN and 17.16 mm, respectively. An interesting feature of this specimen at large displacements was severe damage of the outer course of bricks and buckling of the outermost NSM strip in compression (Fig. 10c) near the mid-span, in the vicinity of the displacement transducer. This made the recorded displacements artificially higher and caused an elongation of the hysteresis loops in the pull direction (Fig. 9f). Another interesting remark is that the failure load of specimen B_NSM3 was reduced compared to B_R1 or B_M1, despite the similar volumetric ratio of carbon fibers in these specimens. This may be attributed to debonding of the NSM strips, which, on the other hand, resulted in more ductile response characteristics.

Overall, it is concluded that textile-reinforced mortar jacketing was extremely effective. If failure is controlled by tensile fracture of the jacket (low reinforcing ratios), the effectiveness of TRM in terms of strength and deformability is slightly less than that of its resin-based counterpart (by approximately 20% and about 15% for strength and displacement at failure, respectively); but if failure occurs in the wall (higher reinforcing ratios), TRM jackets outperform their resin-based counterparts (by 13% and about 40% for strength and displacement at failure, respectively).

By comparison of the cumulative dissipated energies given in Fig. 9h and Table 1, it is concluded that, in general, the energy dissipation capacities of the TRM-based system and its resin-based counterpart are comparable (and slightly higher in the case of TRM). Finally, the comparison of the stiffness versus loading cycles shown also in Fig. 9h confirms the marginally more compliant behavior of TRM-jacketed masonry versus its resin-based counterpart at early stages of deformation, a behavior which reverses at larger deformations, if resin-based strengthened specimens have already failed while their TRM counterparts are still intact.

If compared with either mortar-based or cement-based jacketing, NSM-based strengthening (of similar carbon fiber reinforcing ratios) may offer higher deformability, due to controlled debonding, at the expense of reduced strength, energy dissipation and stiffness.

4 Conclusions

Based on the response of brick masonry wallettes subjected to out-of-plane cyclic bending it is concluded that textile-reinforced mortar overlays provide a substantial gain in strength and deformability; this gain is higher as the number of layers increases. If failure is controlled by damage in the masonry, TRM overlays outperform their FRP counterparts on the basis of maximum load and displacement at failure, whereas if the failure mechanism involves tensile fracture of the textile reinforcement the effectiveness of TRM versus FRP is slightly reduced. NSM reinforcement (at the same fiber reinforcing ratio) is less effective in strength but more effective in deformability than both TRM and FRP overlays, due to controlled debonding of the FRP strips.

From the results obtained in this study the authors believe that TRM jacketing is an extremely promising solution for strengthening and seismic retrofitting of unreinforced masonry subjected to out-of-plane bending. Further investigation is needed in order to enhance the experimental database and to optimize the TRM-based strengthening system.

Acknowledgements The authors wish to thank Mrs. M. Bouzoukou and Mr. C. Bavellas for their assistance in the experimental program. The work reported in this paper was partially funded by the Greek General Secretariat for Research and Technology, through the project ARISTION, within the framework of the program ''Built Environment and Management of Seismic Risk'', and by the European STREP project INCO-CT-2005-517765-OPERHA.

References

1. Coburn AW, Spence RJS (2002) Earthquake protection. 2nd ed., Wiley, Chichester, UK
2. Triantafillou TC, Fardis MN (1997) Strengthening of historic masonry structures with composite materials. Mater Struct 30:486–486
3. Valuzzi MR, Tinazzi D, Modena C (2003) Strengthening of masonry structures under compressive loads by using FRP strips. In: Tan KH (ed) FRPRCS6. 6th international conference on fibre-reinforced plastics for reinforced concrete structures, Singapore, July 2003. World Scientific Publishing Co., Singapore, pp 1249–1258
4. Krevaikas T, Triantafillou TC (2005) Masonry confinement with fiber reinforced polymers. J Compos Constr 9(2):128–135
5. Schwegler G (1994) Masonry construction strengthened with fiber composites in seismically endangered zones. In: Duma G (ed) 10th European conference on earthquake engineering, Vienna, Austria, September 1994. A. A. Balkema, Rotterdam, The Netherlands, pp 454–458
6. Laursen PT, Seible F, Hegemier GA, Innamorato D (1995) Seismic retrofit and repair of masonry walls with carbon overlays. In: Taerwe L (ed) Proceedings of the 2nd international RILEM symposium: non-metallic (FRP) reinforcement for concrete structures, Ghent, Belgium, August 1995. Spon Press, pp 617–623
7. Ehsani MR, Saadatmanesh H, Al-Saidy A (1997) Shear behaviour of URM retrofitted with FRP overlays. J Compos Constr 1(1):17–25
8. Triantafillou TC (1998) Strengthening of masonry structures using epoxy-bonded FRP laminates. J Compos Constr 2(2):96–104
9. Badoux M, Elgwady MA, Lestuzzi P (2002) Earthquake simulator tests on unreinforced masonry walls before and after upgrading with composites. In: Proceedings of the 12th European conference on earthquake engineering, London, UK, September 2002. Elsevier Science Ltd., paper ref. 862
10. Fam A, Musiker D, Kowalsky M, Rizkalla S (2002) In-plane testing of damaged masonry wall repaired with FRP. Adv Compos Lett 11(6):277–283
11. Moon FL, Yi T, Leon RT, Kahn LF (2002) Seismic strengthening of unreinforced masonry structures with FRP overlays and post-tensioning. In: Proceedings of the 12th European conference on earthquake engineering, London, UK, September 2002. Elsevier Science Ltd., paper ref. 613
12. Marcari G, Manfredi G, Pecce M (2003) Experimental behaviour of masonry panels strengthened with FRP sheets. In: Tan KH (ed) FRPRCS6. 6th international conference on fibre-reinforced plastics for reinforced concrete structures, Singapore, July 2003. World Scientific Publishing Co., Singapore, pp 1209–1218
13. Stratford T, Pascale G, Manfroni O, Bonfiglioli B (2004) Shear strengthening masonry panels with sheet glass-fiber reinforced polymer. J Compos Constr 8(5):434–443
14. Krevaikas TD, Triantafillou TC (2005) Computer-aided strengthening of masonry walls using fibre-reinforced polymer strips. Mater Struct 38:93–98
15. Ehsani MR, Saadatmanesh H, Velazquez-Dimas JI (1999) Behaviour of retrofitted URM walls under simulated earthquake loading. J Compos Constr 3(3):134–142
16. Velazquez-Dimas JI, Ehsani MR (2000) Modeling out-of-plane behaviour of URM walls retrofitted with fiber composites. J Compos Constr 4(4):172–181
17. Albert ML, Elwi AE, Cheng R (2001) Strengthening of unreinforced masonry walls using FRPs. J Compos Constr 5(2):76–84

18. Hamilton HR, Dolan CW (2001) Flexural capacity of glass FRP strengthened concrete masonry walls. J Compos Constr 5(3):170–178
19. Hamoush SA, McGinley MW, Mlakar P, Scott D, Murray K (2001) Out-of-plane strengthening of masonry walls with reinforced composites. J Compos Constr 5(3):139–145
20. Kuzik MD, Elwi AE, Cheng JJR (2003) Cyclic flexure tests of masonry walls reinforced with glass fiber reinforced polymer sheets. J Compos Constr 7(1):20–30
21. Ghobarah A, El Mandooh Galal K (2004) Out-of-plane strengthening of unreinforced masonry walls with openings. J Compos Constr 5(3):170–178
22. Tumialan G, Huang P-C, Nanni A, Silva P (2001) Strengthening of masonry walls by FRP structural repointing. In: Burgoyne CJ (ed) FRPRCS5 5th international conference on fibre-reinforced plastics for reinforced concrete structures, Cambridge, UK, July 2001. Thomas Telford, pp 1033–1042
23. Li T, Galati N, Tumialan JG, Nanni A (2005) ''Analysis of unreinforced masonry concrete walls strengthened with glass fiber-reinforced polymer bars.'' ACI Struct J 102(4):569–577
24. Valluzzi MR, Valdemarca M, Modena C (2001) Behavior of brick masonry vaults strengthened by FRP laminates. J Compos Constr 5(3):163–169
25. Foraboschi P (2004) Strengthening of masonry arches with fiber-reinforced polymer strips. J Compos Constr 8(3):191–202
26. ACI 549.2R-04, Report on Thin Reinforced Cementitious Products. ACI Committee 549, American Concrete Institute, Farmington Hills, Michigan, 2004
27. Kolsch H (1998) Carbon fiber cement matrix (CFCM) overlay system for masonry strengthening. J Compos Constr 2(2):105–109
28. Bischoff T, Wulfhorst B, Franzke G, Offermann P, Bartl A-M, Fuchs H, Hempel R, Curbach M, Pachow U, Weiser W (1998) Textile reinforced concrete façade elements – An investigation to optimize concrete composite technologies. In: Proceedings of the 43rd international SAMPE symposium, pp 1790–1802
29. Curbach M, Jesse F (1999) High-performance textile-reinforced concrete. Structural Engineering International IABSE 4:289–291
30. Brameshuber W, Brockmann J, Roessler G (2001) Textile reinforced concrete for formwork elements – Investigations of structural behaviour. In: Burgoyne CJ (ed) FRPRCS5. 5th international conference on fibre-reinforced plastics for reinforced concrete structures, Cambridge, UK, July 2001. Thomas Telford, pp 1019–1026
31. Naaman AE (2003) Progress in ferrocement and textile hybrid composites. In: Curbach M (ed), Proceedings of the 2nd colloquium on textile reinforced structures, Dresden, Germany, September 2003, pp 325–346
32. Reinhardt HW, Krueger M, Grosse CU (2003) Concrete prestressed with textile fabric. Journal of Advanced Concrete Technology 1(3):231–239
33. Curbach M, Brueckner A (2003) Textile strukturen zur querkraftverstaerkung von stahlbetonbauteilen. In: Curbach M (ed), Proceedings of the 2nd colloquium on textile reinforced structures, Dresden, Germany, September 2003, pp 347–360 (in German)
34. Curbach M, Ortlepp R (2003) Besonderheiten des verbundverhaltens von verstaerkungsschichten aus textilbewehrtem. In: Curbach M (ed), Proceedings of the 2nd colloquium on textile reinforced structures, Dresden, Germany, September 2003, pp 361–374 (in German)
35. Brueckner A, Ortlepp R, Weiland S, Curbach M (2005) Shear strengthening with textile reinforced concrete. In: Hamelin P (ed), CCC 2005: 3rd international conference on composites in construction, Lyon, France, July 2005, pp 1307–1314
36. Triantafillou TC, Papanicolaou CG (2005) Textile reinforced mortars (TRM) as strengthening materials for concrete structures. In: Balazs GL, Borosnyoi A (eds) Proceedings of the fib symposium ''keep concrete attractive. Budapest, Hungary, pp 345–350
37. Triantafillou TC, Papanicolaou CG (2006) Shear strengthening of reinforced concrete members with textile reinforced mortar (TRM) jackets. Mater Struct. 39(1): 85–93
38. Triantafillou TC, Papanicolaou CG, Zissimopoulos P, Laourdekis T (2006) Concrete confinement with textile reinforced mortar (TRM) jackets. ACI Structural Journal 103(1):28–37
39. Faella C, Martinelli E, Nigro E, Paciello S (2004) Tuff masonry walls strengthened with a new kind of C-FRP sheet: experimental tests and analysis. In: Proceedings of the 13th world conference on earthquake engineering, paper no. 923
40. Krevaikas T (2005) Strengthening of unreinforced masonry structures with advanced composites. Ph.D. Dissertation, Department of Civil Engineering, University of Patras, Greece (in Greek)
41. Nurchi A, Valdes M (2005) Strengthening of stone masonry columns by means of cement-based composite wrapping. In: Hamelin P (ed), CCC 2005: 3rd international conference on composites in construction, Lyon, France, July 2005, pp 1189–1196
42. Papanicolaou CG, Triantafillou TC, Karlos K, Papathanasiou M (2006) Textile Reinforced Mortar (TRM) versus FRP as strengthening material of URM walls: In-plane Cyclic Loading. Mater Struct, (in press) DOI: 10/1617/s11527-006-9207-8
43. EN 1015-11 (1993). Methods of test for mortar for masonry – Part 11: Determination of flexural and compressive strength of hardened mortar, European Committee for Standardization, Brussels